Dyadic contrast function for the forward model of diffraction tomography of thin cylindrical objects

Tadahiro Negishi, *Student Member, IEEE*, Vittorio Picco, *Member, IEEE*, Lorenzo Lo Monte, *Senior Member, IEEE*, Danilo Erricolo, *Fellow, IEEE*

Abstract—**A forward model for diffraction tomography is derived for the case of thin cylindrical objects by introducing a dyadic contrast function that takes into account depolarization phenomena, which were not previously addressed. As a result, polarimetric measurements may be used to distinguish between dielectric or metallic thin-cylindrical objects. In the case of metallic objects, it is also possible to reconstruct their direction.**

Index Terms—**Inverse Scattering, Diffraction Tomography, Microwave Tomography, RF Tomography, Dyadic contrast function**

I. Introduction

DIFFRACTION Tomography techniques [1]–[4] are widely used in various applications, including detection of underground tunnels (RF Tomography) [5]–[7] and medical imaging (Microwave Tomography) [8].

The forward model of diffraction tomography contains a scalar contrast function, which depends on the permittivity distribution [5].

In this article, the dyadic contrast function is introduced to take into account depolarization effects that may occur when an incident electric field illuminates structures made of thin elongated cylinders. These structures are chosen to both emphasize situations that require the new dyadic contrast function and to simplify the explanation. Incidentally, it is possible to derive a parallel between the new dyadic contrast function and the diffusion tensor imaging used in Magnetic resonance imaging [9].

First, a forward model with a dyadic contrast function is derived by assuming that only thin elongated cylinders exist in a scene. Second, the new forward model using the dyadic contrast function is tested on an inverse scattering problem. The values of the reconstructed dyadic contrast function indicate if depolarization is present or not. When depolarization is present the target is considered metallic, otherwise it is considered made of dielectric material. In addition, the direction of the object may be determined by means of the eigenvalue analysis of the dyadic contrast function. Preliminary results were presented in [10], [11].

II. Depolarization due to elongated cylinders

The electric field scattered by metallic thin cylinder structures shows depolarization effects with respect to the polarization of the incident electric field. Depolarization is essentially absent when the same geometry is made of dieletric material. To visualize this effect, we consider the currents induced on a complex structure composed of many thin cylinders made of metallic or dielectric material, as shown in the Method of Moments results of Fig. 1. This structure is illuminated by an incident plane wave that propagates along the negative x direction and is linearly polarized with the electric field oriented at $45°$ with respect to the z axis on the yz plane.
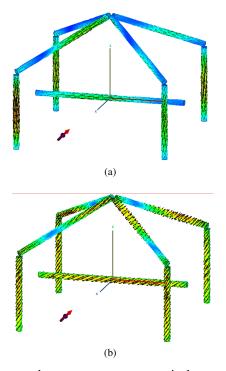

(a)

(b)

Fig. 1: Impressed currents on a geometrical structure made of (a) PEC and (b) dielectric material with $\varepsilon_r = 5$. The polarization of the incident plane wave is indicated by the red arrow.

In the case of a metallic structure, Fig. 1a shows that the direction of the currents is essentially parallel to the direction of the long axes of the structures' elements. In the case of a dielectric material, Fig. 1b shows that the direction of the current is parallel to the direction of the incident electric field.

In order to account for the observed depolarization effects

in complex structures composed of thin cylinders, the forward model used in diffraction tomography is modified with the introduction of the following dyadic contrast function

$$\mathbf{E^s}(\mathbf{r^t}, \mathbf{r^r}) = Q k_0^2 \int_v \hat{\mathbf{a}}^{\mathrm{r}} \cdot \underline{\underline{\mathbf{G}}}(\mathbf{r^r}, \mathbf{r'}) \cdot \underline{\underline{\mathbf{V}}}(\mathbf{r'}) \cdot \underline{\underline{\mathbf{G}}}(\mathbf{r'}, \mathbf{r^t}) \cdot \hat{\mathbf{a}}^{\mathrm{t}} d\mathbf{r'},$$
(1)

where $\mathbf{r^t}$ and $\mathbf{r^r}$ are the locations of the transmitter and receiver antennas; $\hat{\mathbf{a}}^{\mathrm{t}}$ and $\hat{\mathbf{a}}^{\mathrm{r}}$ represent the direction of the transmitter and receiver antennas, which are assumed to be small dipoles; $Q = j\omega\mu_0\Delta\ell^t I^t$ for small dipoles; and, $\underline{\underline{\mathbf{G}}}$ is the dyadic Green's function for the homogeneous space. The dyadic contrast function $\underline{\underline{\mathbf{V}}}$ is

$$\underline{\underline{\mathbf{V}}}(\mathbf{r'}) = \begin{pmatrix} V_{xx} & V_{xy} & V_{xz} \\ V_{yx} & V_{yy} & V_{yz} \\ V_{zx} & V_{zy} & V_{zz} \end{pmatrix}.$$
(2)

In the case of a dielectric elongated thin cylinder, the dyadic contrast function essentially behaves as

$$\underline{\underline{\mathbf{V}}}(\mathbf{r'}) = [\varepsilon(\mathbf{r'}) - \varepsilon_b] \, \mathbf{I},$$
(3)

while in the case of a metallic thin elongated cylinder,

$$\underline{\underline{\mathbf{V}}}(\mathbf{r'}) = -j\frac{\sigma(\mathbf{r'})}{\omega\varepsilon_0}\hat{\mathbf{u}}_{\mathbf{1}}^t\hat{\mathbf{u}}_{\mathbf{1}},$$
(4)

where $\hat{\mathbf{u}}_{\mathbf{1}}$ is a unit vector parallel to the direction of the long axis of the thin cylinder. Additional insights to understand the meaning of the dyadic contrast function may be obtained by individually analyzing the elements of Eq. (1) proceeding from right to left. The term $\underline{\underline{\mathbf{G}}}(\mathbf{r'}, \mathbf{r^t}) \cdot \hat{\mathbf{a}}^{\mathrm{t}}$ has the meaning of incident electric field in the domain v:

$$\tilde{\mathbf{E}}^{\mathrm{i}} = \underline{\underline{\mathbf{G}}} \cdot \hat{\mathbf{a}}^{\mathrm{t}} = \begin{bmatrix} E_x^{\mathrm{i}} \\ E_y^{\mathrm{i}} \\ E_z^{\mathrm{i}} \end{bmatrix} = \begin{bmatrix} G_{xx}a_x^t + G_{xy}a_y^t + G_{xz}a_z^t \\ G_{yx}a_x^t + G_{yy}a_y^t + G_{yz}a_z^t \\ G_{zx}a_x^t + G_{zy}a_y^t + G_{zz}a_z^t \end{bmatrix}.$$
(5)

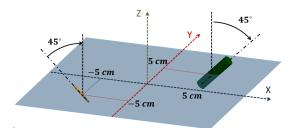The incident field then multiplies the dyadic contrast function,

Fig. 2: Geometry for example. There are a thin PEC at (-5, -5) cm and a thicker dielectric cylinders at (5, 5) cm which intersect the xy plane at a 45° angle.

and an equivalent impressed surface current term is obtained

$$\tilde{\mathbf{J}} = \underline{\underline{\mathbf{V}}} \cdot \tilde{\mathbf{E}}^{\mathrm{i}} = \begin{bmatrix} J_x \\ J_y \\ J_z \end{bmatrix} = \begin{bmatrix} V_{xx}E_x^{\mathrm{i}} + V_{xy}E_y^{\mathrm{i}} + V_{xz}E_z^{\mathrm{i}} \\ V_{yx}E_x^{\mathrm{i}} + V_{yy}E_y^{\mathrm{i}} + V_{yz}E_z^{\mathrm{i}} \\ V_{zx}E_x^{\mathrm{i}} + V_{zy}E_y^{\mathrm{i}} + V_{zz}E_z^{\mathrm{i}} \end{bmatrix}.$$
(6)

It is evident that while a scalar contrast function produces an impressed current $\tilde{\mathbf{J}}$ which is always parallel to $\tilde{\mathbf{E}}^{\mathrm{i}}$, a dyadic contrast function can correctly represent depolarization effects due to its off-diagonal terms. This equivalent current produces a scattered field through the Green's function, which is projected onto the receiving antenna direction.

To simplify the notation, the auxiliary row vector $\mathbf{p}$ is introduced

$$\mathbf{p} = \hat{\mathbf{a}}^{\mathrm{r}} \cdot \underline{\underline{\mathbf{G}}} = \begin{bmatrix} p_x \\ p_y \\ p_z \end{bmatrix}^T = \begin{bmatrix} a_x^r G_{xx} + a_y^r G_{yx} + a_z^r G_{zx} \\ a_x^r G_{xy} + a_y^r G_{yy} + a_z^r G_{zy} \\ a_x^r G_{xz} + a_y^r G_{yz} + a_z^r G_{zz} \end{bmatrix}^T.$$
(7)

Overall, for a given combination of locations of the transmitter at $\mathbf{r^t}$, receiver at $\mathbf{r^r}$, and their respective polarizations $\hat{\mathbf{a}}^{\mathrm{t}}$ and $\hat{\mathbf{a}}^{\mathrm{r}}$, the contribution to the scattered field E^s due to a scatterer at $\mathbf{r'}$ can be written as

$$\begin{aligned} dE^s = \mathbf{p} \cdot \tilde{\mathbf{J}} &= p_x J_x + p_y J_y + p_z J_z \\ &= p_x \left(V_{xx}E_x^{\mathrm{i}} + V_{xy}E_y^{\mathrm{i}} + V_{xz}E_z^{\mathrm{i}} \right) \\ &+ p_y \left(V_{yx}E_x^{\mathrm{i}} + V_{yy}E_y^{\mathrm{i}} + V_{yz}E_z^{\mathrm{i}} \right) \\ &+ p_z \left(V_{zx}E_x^{\mathrm{i}} + V_{zy}E_y^{\mathrm{i}} + V_{zz}E_z^{\mathrm{i}} \right) d\mathbf{r'}. \end{aligned}$$
(8)

The previous expression is conveniently recast as the scalar product of a 9 element vector $\boldsymbol{\ell}$, containing all the known terms, and of a vector $\mathbf{t}$, containing the 9 unknown elements of the dyadic contrast function, i.e. $dE^s = \boldsymbol{\ell}\mathbf{t}d\mathbf{r'}$, where

$$\boldsymbol{\ell} = [p_x E_x^i, p_x E_y^i, p_x E_z^i, p_y E_x^i, p_y E_y^i, p_y E_z^i, p_z E_x^i, p_z E_y^i, p_z E_z^i],$$
(9)

$$\mathbf{t} = [V_{xx}, V_{xy}, V_{xz}, V_{yx}, V_{yy}, V_{yz}, V_{zx}, V_{zy}, V_{zz}]^T.$$
(10)

The domain of investigation v is discretized into P pixels, so that there is a total number of $9P$ unknowns. For each measurement, it is possible to consider up to 9 linearly independent combinations for the polarization of the transmitter and the receiver. Assuming a number m of transmitters and a number n of receivers, the maximum number of measurements is $9mn$. Then, a matrix $\mathbf{L}$ is constructed so that each row corresponds to one possible combination of position and polarization of the transmitter and the receiver, while each pixel location is associated to 9 columns of $\mathbf{L}$ so that overall the matrix $\mathbf{L}$ has $9mn$ rows and $9P$ columns. A column vector $\mathbf{T}$ is constructed by appending the vectors $\mathbf{t}$ for each pixel, for a total of $9P$ elements. In the end, one obtains the equation

$$\mathbf{E^s} = \mathbf{LT}.$$
(11)

The forward model obtained in eq. (11) must be inverted to obtain the dyadic contrast function. The matrix L is normally ill-conditioned, therefore regularized inversion methods of either direct (e.g. Truncated Singular Value Decomposition) or iterative (e.g. Conjugate Gradient, Algebraic Reconstruction Technique) type must be used.

III. SOLUTION OF THE INVERSE PROBLEM

The dyadic contrast function is computed for the sample geometry shown in Fig. 2. It is assumed that 21 infinitesimal dipole transmitters and 40 receivers are placed in the $z = 0$ plane, and are uniformly distributed along two concentric circles centered at the origin with a radius of 44.5 cm for
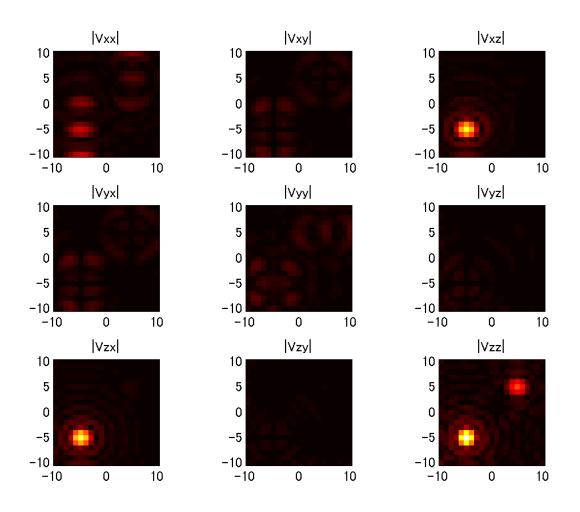
Fig. 3: The 9 reconstructed components of the dyadic contrast function for the sample geometry of Fig. 2.

the transmitters and 23.1 cm for the receivers. Criteria for the optimal number and locations of transmitters and receivers are discussed in [12] and references therein. All three orthogonal polarizations for each individual transmitter and receiver are considered. Overall, $21 \times 40 \times 9 = 7560$ measurements are collected. The scattered field is computed by Method of Moment simulations through the commercial computational electromagnetic software FEKO. The frequency of operation is 3.16 GHz ($\lambda \approx 9.5$ cm).

In this example, a thin metallic cylinder and a thicker dielectric cylinder, with $\varepsilon_r = 1.5$, exist in the volume under investigation and are shown in orange and green respectively. The metallic cylinder, which has a radius of 1 mm and is 2 cm long, is centered at (-5, -5) cm in the $z = 0$ plane, its axis is located in the xz plane and makes a -45 degree angle with the z axis. The dielectric cylinder, which has a radius of 5 mm and is 4 cm long, is centered at (5, 5) cm in the z=0 plane, its axis is located in the xz plane and makes a 45 degree angle with the z axis. The dielectric cylinder is intentionally chosen bigger than the metallic cylinder so that the corresponding scattered field is stronger and is not masked by the field scattered by the metallic cylinder.

The area under investigation is colored in blue and is square with a side of 20 cm in length and is centered at the origin. The area is partitioned into pixels of size $\lambda/10$. This corresponds to a total of $21 \times 21 \times 9 = 3969$ unknowns.

The conjugate gradient method is used in the inversion of eq. (11) to retrieve the vector $\mathbf{T}$. Then, the elements of the vector $\mathbf{T}$ are rearranged so as to create 9 reconstructed images versions, each one corresponding to a different component of dyadic contrast $\underline{\underline{\mathbf{V}}}$. The results were computed using a laptop computer with Intel® Core™ i7-3610QM @2.30 GHz CPU. The computational time was 52.3 seconds for creating the model $\mathbf{L}$, and 4.1 seconds for the inversion.

A. 9 components of dyadic contrast

The result of the inversion for the example under consideration can be visualized as a 3-by-3 collection of images and are shown in Fig. 3. For the thin metallic cylinder, which is located at (-5 ,-5) cm, the components of the dyadic contrast function that are different from zero are the diagonal terms xx, and zz and the off-diagonal terms xz and zx. The presence of the off-diagonal terms indicates strong depolarization, which is a signature of a elongated cylindrical metallic object. On

the other hand, for the dielectric cylinder, which is located at (5, 5) cm the components of the dyadic contrast function that are different from zero are only the diagonal terms xx and zz. The lack of strong off-diagonal terms is a signature of an elongated cylindrical dielectric object.

Fig. 3 also shows that the zz component is stronger than the other ones. This is due to the pattern of the antennas. In fact, since the small dipoles are placed in the xy plane, only when both transmitter and receiver are oriented along the $\hat{z}$ direction there are no radiation pattern nulls pointing towards the object. All other polarizations are affected by the presence of nulls and therefore produce a weaker response.

B. Eigenvalues-eigenvectors analysis

In the case of metallic elongated cylinders, the eigenvector analysis of the dyadic contrast funtion leads to the determination of the direction of the long axis of the cylinder. In fact, due to the depolarization, the largest eigenvalue is associated with the eigenvector parallel to the long axis of the cylinder. So, assuming that there is depolarization, let $\mathbf{u_1}$ be the eigenvector associated with the largest eigenvalue λ_1 of the contrast function. Then, consider the vector

$$\mathbf{d} = \lambda_1 \mathbf{u_1} \tag{12}$$

which is displayed in the region of interest as a quiver plot and is shown in Fig. 4. Two types of information are obtained: (i) the location of the target through the magnitude of $\mathbf{d}$ and (ii) the direction of the cylinder through the direction of $\mathbf{d}$. The quiver plot should be interpreted in this way: (i) an object is located where the magnitude of the arrows is large and (ii) the direction of an object is indicated by the orientation of the arrows in the 3D space. The same result obtained in Fig. 3 can be processed with the eigen-decomposition.
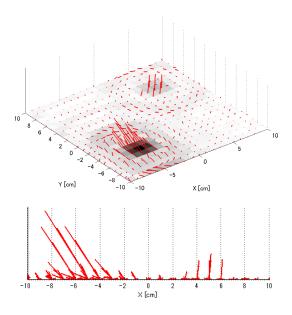

Fig. 4: Quiver plot obtained with eigendecomposition. The gray image is the absolute value of the sum of all components of the image. Two views are provided.

The reconstructed vectors $\mathbf{d}$ result into arrows oriented at an angle $\theta = 32°$ in the same direction as the thin elongated metallic cylinder $\mathbf{t}$ at (-5, -5) cm. On the other hand, the arrows point toward the $\hat{z}$ direction for the dielectric cylinder. The resulting vectors tend to point toward the $\hat{z}$ direction due to the strong V_{zz} component, and this specific measurement configuration.

IV. CONCLUSION

The anisotropic forward model using dyadic contrast function is derived to represent depolarization for thin metallic cylinders. The dyadic contrast allows to observe if depolarization exists and the off-diagonal components of the dyadic contrast function can be used to determine whether objects are metallic or dielectric. The direction of a thin metallic cylinder is given by the direction of the eigenvector associated with the largest eigenvalue of the dyadic contrast function. As future work, the new model can be extended to reconstruct surfaces of more general objects made of metal by considering the first two largest eigenvalues of $\underline{\mathbf{V}}$. The expected difficulty is that the current distribution on the object is no longer a linear function of the the incident field.

REFERENCES

[1] M. Zhdanov, *Geophysical electromagnetic theory and methods*. Elsevier Science Ltd., 2009.
[2] M. Pastorino, *Microwave Imaging*. John Wiley & Sons, April 2010.
[3] T. J. Cui, W. C. Chew, X. X. Yin, and W. Hong, "Study of resolution and super resolution in electromagnetic imaging for half-space problems," *IEEE Trans. Antennas Propag.*, vol. 52, no. 6, pp. 1398–1411, June 2004.
[4] R. Firoozabadi, E. L. Miller, C. M. Rappaport, and A. W. Morgenthaler, "Subsurface sensing of buried objects under a randomly rough surface using scattered electromagnetic field data," *IEEE Trans. Geosci. Remote Sensing*, vol. 45, no. 1, pp. 104–117, Jan 2007.
[5] L. Lo Monte, D. Erricolo, F. Soldovieri, and M. Wicks, "Radio Frequency Tomography for Tunnel Detection," *IEEE Trans. Geosci. Remote Sensing*, vol. 48, no. 3, pp. 1128–1137, March 2010.
[6] C. Gilmore, P. Mojabi, A. Zakaria, S. Pistorius, and J. LoVetri, "On super-resolution with an experimental microwave tomography system," *IEEE Antennas Wirel. Propag. Lett.*, vol. 9, pp. 393–396, 2010.
[7] V. Picco, T. Negishi, S. Nishikata, D. Spitzer, and D. Erricolo, "RF Tomography in Free Space: Experimental Validation of the Forward Model and an Inversion Algorithm Based on the Algebraic Reconstruction Technique," *International Journal of Antennas and Propagation*, vol. 2013, article ID 528347, doi:10.1155/2013/528347.
[8] Z. Q. Zhang and Q. H. Liu, "Three-dimensional nonlinear image reconstruction for microwave biomedical imaging," *IEEE Trans. Biomed. Eng.*, vol. 51, no. 3, pp. 544 –548, March 2004.
[9] P. J. Basser and D. K. Jones, "Diffusion-tensor MRI: theory, experimental design and data analysis–a technical review," *NMR in Biomedicine*, vol. 15, no. 7-8, pp. 456–467, 2002.
[10] V. Picco, "Dyadic Contrast Function And Quadratic Forward Model For Radio Frequency Tomography," Ph.D. dissertation, University of Illinois at Chicago, Chicago, IL, May 2014.
[11] V. Picco, T. Negishi, D. Erricolo, and L. L. Monte, "Dyadic Contrast Function for RF Tomography: Preliminary Results," in *2014 IEEE International Conference on Antenna Measurements & Applications*, Antibes Juan-les-Pins, France, Nov. 16-19 2014.
[12] G. Gennarelli, I. Catapano, F. Soldovieri, and R. Persico, "On the Achievable Imaging Performance in Full 3-D Linear Inverse Scattering," *IEEE Trans. Antennas Propag.*, vol. 63, no. 3, pp. 1150–1155, March 2015.